



CHALMERS
UNIVERSITY OF TECHNOLOGY

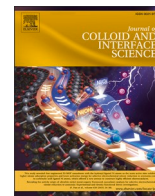
Vertical graphene nanoarray decorated with Ag nanoparticles exhibits enhanced antibacterial effects

Downloaded from: <https://research.chalmers.se>, 2025-06-02 10:32 UTC

Citation for the original published paper (version of record):

Zhang, J., Pandit, S., Rahimi, S. et al (2024). Vertical graphene nanoarray decorated with Ag nanoparticles exhibits enhanced antibacterial effects. *Journal of Colloid and Interface Science*, 676: 808-816.
<http://dx.doi.org/10.1016/j.jcis.2024.07.173>

N.B. When citing this work, cite the original published paper.

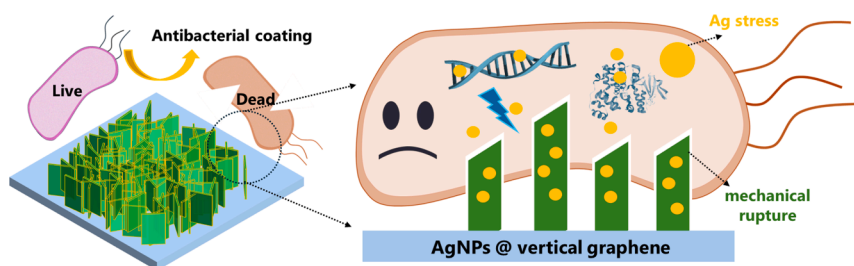


Regular Article

Vertical graphene nanoarray decorated with Ag nanoparticles exhibits enhanced antibacterial effects

Jian Zhang^a, Santosh Pandit^{a,*}, Shadi Rahimi^a, Zhejian Cao^a, Ivan Mijakovic^{a,b,**}^a Systems and Synthetic Biology Division, Department of Life Sciences, Chalmers University of Technology, SE-412 96 Gothenburg, Sweden^b The Novo Nordisk Foundation, Center for Biosustainability, Technical University of Denmark, DK-2800 Kongens Lyngby, Denmark

GRAPHICAL ABSTRACT



ARTICLE INFO

Keywords:

Vertical graphene
Polydopamine
Ag nanoparticles
Antibacterial properties
Cytotoxicity

ABSTRACT

Bacterial infection of biomedical implants is an important clinical challenge, driving the development of novel antimicrobial materials. The antibacterial effect of vertically aligned graphene as a nanoarray coating has been reported. In this study, vertically aligned graphene nanosheets decorated with silver nanoparticles were fabricated to enhance antibacterial effectiveness. Vertically aligned graphene (VG) nanoflakes were synthesized by plasma-enhanced chemical vapor deposition (PECVD). Ag nanoparticles were attached to the surface of VG through polydopamine and achieving a sustained release of Ag^+ . VG loaded with Ag nanoparticles (VGP/Ag) not only prevented bacterial adhesion for a long time, but also exhibited good biocompatibility. This work provides a new venue for designing antibacterial surfaces based on combination of graphene nanoarrays with other nanomaterials, and the results indicate that this approach could be very successful in preventing implant associated infections.

1. Introduction

Biofilm is an important factor causing medical implant infection [1]. The extracellular polymeric substances (EPS) produced by microcolonies can impede the penetration of antibiotics into biofilms and

trigger enzymatic modification or inactivation of antibiotics. The formation of biofilms can lead to increased antibiotic resistance of bacterial strains. Compared with planktonic bacteria, the challenge of biofilm inhibition and surface protection is considerably greater [2]. For the biofilm attachment on medical implant and devices, the introduction of

* Corresponding author.

** Corresponding author at: Systems and Synthetic Biology Division, Department of Life Sciences, Chalmers University of Technology, SE-412 96 Gothenburg, Sweden.

E-mail addresses: pandit@chalmers.se (S. Pandit), ivan.mijakovic@chalmers.se (I. Mijakovic).<https://doi.org/10.1016/j.jcis.2024.07.173>

Received 13 May 2024; Received in revised form 16 July 2024; Accepted 21 July 2024

Available online 22 July 2024

0021-9797/© 2024 The Author(s). Published by Elsevier Inc. This is an open access article under the CC BY license (<http://creativecommons.org/licenses/by/4.0/>).

antimicrobial coatings is seen as a very effective approach to endow implants with excellent antimicrobial properties [3,4]. Interestingly, nanotechnology is showing increasing potential and feasibility in the treatment of antibiotic resistant infections [5]. Emerging two-dimensional (2D) nanomaterials have excellent physical and chemical properties and are widely used in fields such as energy conversion [6–8], optoelectronic devices [9,10] and biomedicine [11], becoming a research hotspot. Graphene and its derivatives such as graphene oxide (GO) have emerged as potential two-dimensional carbon materials to design coatings for biomedical applications, playing an important role in combating device-associated infections [12–15]. The preparation of graphene coatings varies with the substrate materials and the antibacterial effect depends critically on the mechanism of the coatings. Graphene coatings are available in horizontal and vertical arrangements. Horizontally oriented graphene coatings can be produced by chemical vapor deposition (CVD) [16–18]. Horizontal graphene-based coatings can also be achieved by assembling GO on the surface, using approaches such as spin coating, vacuum filtration, electrophoretic deposition and chemical crosslinking [15,19]. Vertically aligned graphene layers are usually produced by plasma-enhanced CVD (PECVD) [20,21]. At high temperatures, when plasma is applied to the sample, gas molecules (carbon source) near the surface are ionized, and carbon grows vertically from the surface, forming a thin layer. Furthermore, Lu et al. used a magnetic field to vertically align GO flakes in a 2-hydroxyethyl methacrylate polymer film [22]. Akhavan et al. produced GO nanowalls with sharp edges were produced by electrophoretic deposition on stainless steel [23].

Potential antimicrobial mechanisms of graphene include physical damage to bacteria cell membranes by sharp edges of graphene sheets, oxidative stress and isolation by wrapping [24–26]. The inherent antibacterial activities of graphene are related to the surface morphology, the degree of interaction of graphene with cells, and the sensitivity of the strains used in the assay [27,28]. The horizontal coating reduces the possibility of direct interaction between graphene edges and bacteria, thus barely disrupt the bacterial cell membrane. In addition to that such coatings do not readily encapsulate and sequester bacterial cells. In contrast, vertically aligned graphene has attracted interest as an antimicrobial coating. Vertically aligned graphene has exposed sharp edges that are critical for bacterial toxicity. The sharp edges of the graphene flake coating disrupt the bacterial membrane when in direct physical contact. Graphene can extract phospholipid molecules from the lipid layer of the cell membrane, triggering deformation and irreversible damage of cell membranes, resulting in bacterial inactivation [29,30]. In addition to physical effects, the oxidative stress generated by the interaction between the graphene and microorganisms can trigger redox reaction with cellular components such as DNA, lipids, and proteins [31–33]. Both of killing mechanisms are unlikely to induce the bacterial resistance, making vertically aligned graphene coatings promising against drug resistant pathogen biofilms. In addition, vertical graphene exhibits excellent biocompatibility. Wei et al. confirmed that vertically deposited graphene does not exhibit cytotoxicity towards human adipose-derived stem cells (hADSCs), and hADSCs are able to continually proliferate thereon [34]. Similarly, Pandit et al. reported that Silicon surfaces coated with vertical graphene showed no discernible impact on the viability of mouse fibroblasts (NIH3T3) and human neuroblastoma cells (SH-SY5Y) [35]. Zhang et al. developed vertical graphene coatings on titanium and demonstrated no significant cytotoxic effects on osteoblast MC3T3-E1 cells [36].

The study of antimicrobial properties of graphene is an emerging area, with several reports of vertical graphene preventing early bacterial adhesion and biofilm formation. Surface functionalization and loading of vertical graphene with drugs to enhance its antimicrobial properties is an unexplored area with considerable potential. Composite antimicrobial coatings based on vertical graphene have not been investigated. Antimicrobial studies of vertical graphene so far mainly focused on short periods, of up to 24 h. Thus, the long-term durability of graphene

coatings in antimicrobial applications needs to be investigated. Although the biocompatibility of vertical graphene has been confirmed by previous studies, the toxicity of composite antimicrobial coatings is often a challenge for their implementation. In this study, we developed a composite antimicrobial coating utilizing vertical graphene (VG). It involved the fabrication of VG using PECVD, followed by functionalization with Ag nanoparticles via mussel-inspired polydopamine (PDA), while preserving the vertical orientation of graphene. The PDA was covalently formed on VG by self-polymerizing its monomer dopamine [37,38]. Ag nanoparticles were reduced and stabilized within the layer through catechol-Ag⁺ chemical reactions [39]. The pathogenic bacteria *Escherichia coli* was used as models to evaluate the antimicrobial activity, longevity, and mechanism of the coatings. MG-63 osteoblastic-like human cells were used to examine biocompatibility of the coatings. The results show that the composite coating made of Ag nanoparticles and VG is very effective in inhibiting pathogenic biofilms.

2. Experimental sections

2.1. Bacterial strains, chemicals, and materials

E. coli (UTI89) were obtained from Gothenburg University Culture Collection (CCUG) and used for evaluation of antibacterial efficiency of VG samples. Luria–Bertani (LB) broth (Lennox) was bought from Sigma-Aldrich (Sweden). Silver nitrate (ACS reagent, ≥99.0 %), sodium chloride (ACS reagent, ≥99.0 %), tris(hydroxymethyl)aminomethane (Primary Standard and Buffer, ≥99.9 %) and dopamine hydrochloride were purchased from Sigma-Aldrich (Sweden). All of the chemicals were used without further purification.

2.2. Synthesis of vertical graphene

Vertical graphene (VG) was synthesized on SiO₂ using plasma-enhanced chemical vapor deposition (PECVD) with the Axitron Black Magic system. The SiO₂ substrate consisted of a silicon wafer with a 400 nm thick SiO₂ film. The experimental process involved loading the substrate into a cold wall CVD system. The samples were then rapidly heated at a rate of 300 °C per minute until reaching the desired growth temperature of 775 °C. For one minute, the samples were annealed with a mixture of 20 sccm H₂ gas and 1000 sccm Ar gas. Subsequently, the plasma was activated under a DC bias of 75 W. The growth of vertical graphene was initiated by introducing a gas mixture comprising 15 sccm C₂H₂, 15 sccm H₂ and 1000 sccm Ar, which was maintained for 15 min. After the growth, the system was evacuated to a pressure below 0.2 mbar and subsequently cooled down.

2.3. Polydopamine-mediated loading of Ag nanoparticles

The VG coating was initially functionalized with polydopamine (PDA). VG samples were immersed in a freshly prepared solution of dopamine hydrochloride (2 mg/mL) in 10 mM Tris buffer (pH 8.5) for 6 h with gentle shaking. The VG obtained after PDA modification was labeled as VGP. Afterward, the VGP samples were immersed in a solution of 30 mM AgNO₃ for 6 h under dark conditions. Subsequently, the sample was exposed to ultraviolet light for 1 h to further reduce Ag nanoparticles. The VGP samples after Ag nanoparticles loading were labeled as VGP/Ag.

2.4. Characterizations

The characterizations of VG, VGP and VGP/Ag were used by atomic force microscopy (AFM), Fourier-transform infrared (FTIR) spectra, Raman spectra X-ray photoelectron spectroscopy (XPS) and field emission scanning electron microscopy (SEM), which were performed as previously described [14].

2.5. Silver ion release

The release of Ag ions from the VGP/Ag samples were observed under conditions of pH 7.4 in phosphate-buffered saline (PBS) at 37 °C. Each sample underwent immersion in 1 mL of PBS, subsequent removal, and then re-immersion in 1 mL of fresh PBS. This cycle continued for 7 days, yielding solutions at various intervals to chart the time course of silver ion release. Analysis of the silver ion release profiles was conducted by subjecting the PBS solutions containing the released ions to inductively coupled plasma-mass spectrometry (ICP-MS) using a Thermo iCAP Q instrument.

2.6. Antibacterial assays

The *Escherichia coli* (*E. coli*) UTI89 strains were used to evaluate the antibacterial activity by means of agar plate counting. The inoculum ($2\text{--}5 \times 10^6$ CFU/mL) was applied to the VGP/Ag surfaces and incubated at 37 °C under static conditions. After 24 h, the inoculum was removed, and the surfaces were rinsed with sterile H₂O to remove loosely attached bacterial cells. Next, bacteria were collected from VGP/Ag by adding 5 mL of 0.89 % NaCl and homogenizing the suspension through sonication. The homogenized bacterial suspension was then serially diluted in 0.89 % NaCl, and the dilutions were plated on agar plates. These plates were then incubated at 37 °C for 24 h, following which the number of bacterial colonies was counted. The plates were incubated at 37 °C for 24 h, after which the number of bacterial colonies was counted. The antibacterial efficiency (R_a) was calculated using the following formula: $R_a (\%) = (A - B)/A \times 100$, where A and B represent the number of viable bacteria on the SiO₂ and VGP/Ag (VG) specimens, respectively. To study the longevity of the antibacterial activity of the VGP/Ag, additional VGP/Ag specimens were prepared by immersing them in PBS (pH 7.4) at 37 °C for predetermined time intervals (1, 3, 5, 7, and 10 days). These samples were then analyzed using the same protocol as described above, and the R_a values were determined to assess the effectiveness of the coatings in inhibiting biofilm formation. In addition, live/dead staining assay and SEM images were used to visualize the biofilms on VGP/Ag specimens, which were performed as previously described [14,35].

The antibacterial activity of VGP/Ag was studied under long-term culture conditions. The inoculum ($2\text{--}5 \times 10^7$ CFU/mL) was applied to the VGP/Ag. Fresh inoculum was replaced daily to ensure continuous bacterial challenge. After incubating for 1, 3 and 5 days, the bacteria were collected from the VGP/Ag by adding 5 mL of 0.89 % NaCl and homogenizing the suspension through sonication. The homogenized suspension was then serially diluted in 0.89 % NaCl and were plated on agar plates. The plates were incubated at 37 °C for 24 h, after which the number of bacterial colonies was counted.

2.7. Biocompatibility

The experiment was performed with MG-63 cells. Cell lines were maintained at 37 °C with 5 % CO₂ in Minimum Essential Medium Eagle (Thermo Scientific) supplemented with 10 % fetal bovine serum (Thermo Scientific). Cells were seeded onto 48 well plates at a density of 4×10^4 per well in 400 μ L volume and cultured for 24 h in the presence of samples. Then, the samples with the cells on the top were stained and incubated with 1 \times alamarBlue for 3 h at 37 °C. Cell signals were detected via an FLUOStar Omega plate reader, with subsequent normalization of results to the control sample. The cells were seeded into petri dishes at a density of 3×10^5 cells per petri dish in 3 mL volume and cultured for 24 h in the presence of samples. The petri dish without any sample was considered as the negative control. Then, the cells were washed two times with Hanks' Balanced Salt solution (Thermo Scientific) and SYTOX Green (Thermo Scientific) at 1 μ M concentration was added to the cells and incubated at 37 °C for 30 min. Then the cells were washed with Hanks' Balanced Salt solution and imaged using 40 \times objective in LeicaCTR4000 inverted fluorescent microscope. The GFP

filter was used for imaging. For SEM imaging, the cells were seeded into petri dishes at a density of 3×10^5 cells per petri dish in 3 mL volume and cultured for 24 h in the presence of samples. Following treatment, cells underwent PBS washes and were then fixed in 3 % glutaraldehyde for 2 h. Subsequently, the fixed samples underwent dehydration via a series of washes with ascending ethanol concentrations (40 %, 50 %, 60 %, 70 %, 80 %, 90 %, and 100 %), each lasting 10 min, followed by air-drying for 2 h at room temperature.

2.8. Statistical analysis

All measurements were performed in triplicate under the same conditions. All data were expressed as mean \pm standard deviations. A one-way analysis of variance (ANOVA) with a post hoc multiple comparison (Tukey) test was used. The difference between groups * $P < 0.05$ and ** $P < 0.01$ was defined as statistically significant.

3. Results and discussion

VG coatings immobilized with Ag nanoparticles were produced as described in the Experimental section. SEM and AFM images of the surface showcased the uniform structure of vertical graphene nanoflakes, as shown in Fig. 1. Generally, the growth mechanism of VG by PECVD includes three steps: nucleation, vertical growth, and saturation. First, a horizontal buffer layer containing mismatches and curved areas forms on the substrate. From these nucleation sites, vertical graphene begins to grow continuously at the open edges and defects through carbon deposition. Finally, as vertical growth reaches saturation, new branches of flakes tend to emerge from the eroded areas of the main spikes due to plasma etching, resulting in a cluster structure with exposed defects [33,40]. The VG showed a network of standing spiky flakes with the feature of sharp edges (Fig. 1a), which is expected for standard VG growth. Cross-sectional SEM was used to observe the orientation of graphene nanoflakes (Fig. S1). The results showed that the graphene flakes had a partially vertical orientation relative to the substrate. The nanoflake dimensions revealed that the vertical graphene averaged 60 nm in size on the substrate. The root mean square roughness (RMS) value of VG was 25.4 nm. After the PDA was loaded, the surface morphology of VGP did not change significantly (Fig. 1b). The RMS value was decreased to 21.2 nm, indicating the uniform loading of the PDA on the VG surface [41]. Further, after the Ag nanoparticles modification, dispersed Ag nanoparticles were anchored onto the VGP surfaces (Fig. 1c). This did not alter the morphology of the network of standing graphene flakes. The RMS value of VGP/Ag increased, reflecting the attachment of Ag nanoparticles. Additional SEM images and three-dimensional AFM images of VG, VGP and VGP/Ag samples are shown in Fig. S2. EDS mapping of VGP/Ag (Fig. S3) confirmed the presence of C, O, N, and Ag elements, which were evenly distributed within the modified surfaces.

Raman spectroscopy was used to study the hybrid structure of the as-prepared species. Fig. 2a shows the Raman spectrum with characteristic peaks. The three main characteristic Raman peaks for graphene, D, G, and 2D, are all detected. The D peak (1350 cm^{-1}) indicates the presence of disorders. The G peak (1590 cm^{-1}) is related to the $\text{sp}^2 \text{C—C}$ bond and signifies the degree of graphitization. The intensity of the 2D peak (2650 cm^{-1}) decreases with an increasing number of graphene layers and decreasing lattice quality [20,42]. Due to the vertical structure and the large number of flake boundaries and defects, the D band is high compared to the G band. A small 2D peak is observed, indicating that the samples are multilayer graphene [33]. The I_D/I_G ratio of the VG composite is 1.17. Moreover, after PDA functionalization and Ag nanoparticles modification, the I_D/I_G ratios of VGP and VGP/Ag were increased to 1.22. This suggests an increase in defects and the formation of $\pi\text{--}\pi$ bonds between graphene and PDA [43].

Fig. 2b displays the full XPS spectra of VG, VGP and VGP/Ag. The atomic percentages of VG, VGP and VGP/Ag are shown in Table S1. The

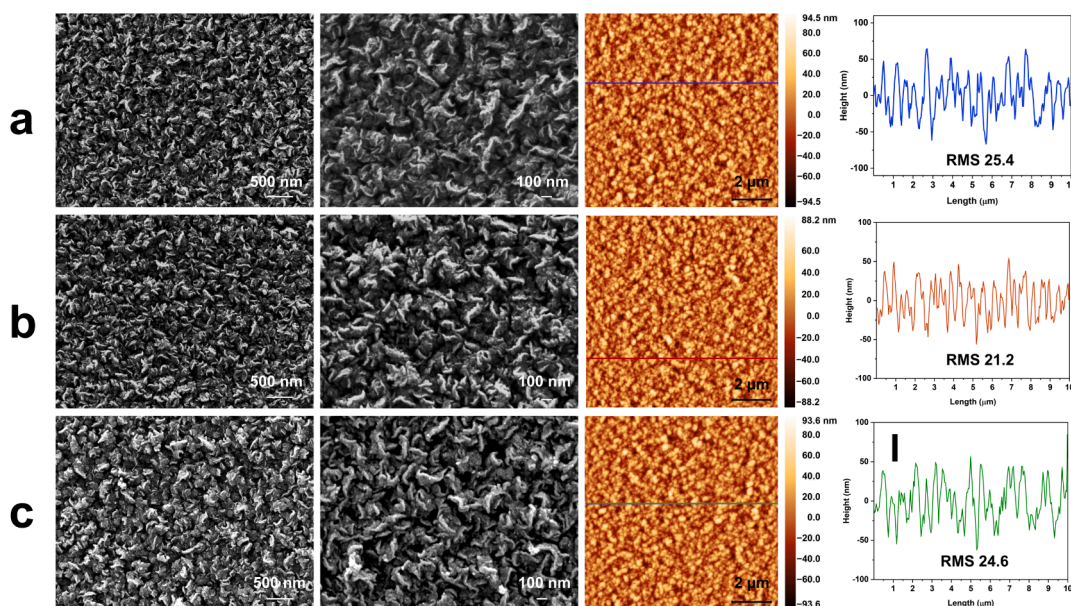


Fig. 1. SEM images, AFM images and the correspondence cross-sectional profiles extracted from AFM images of VG (a), VGP (b) and VGP/Ag (c).

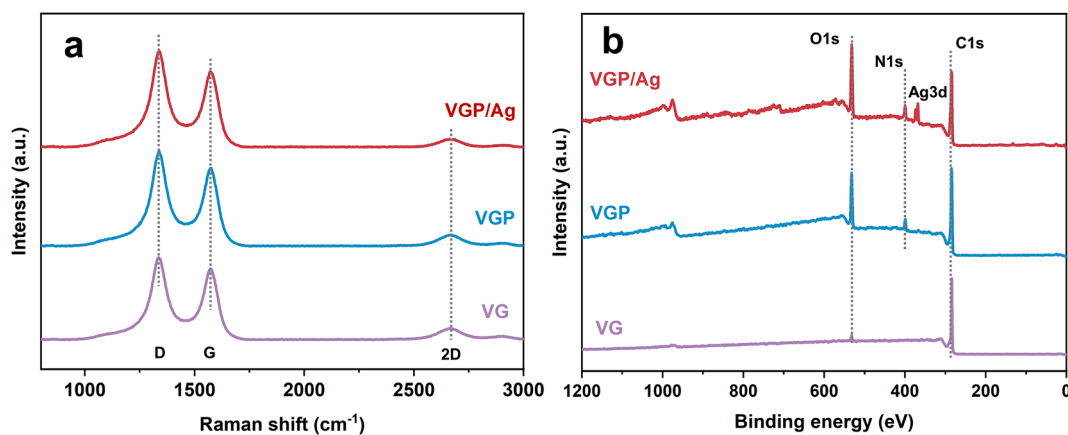


Fig. 2. Raman spectra (a) and full scan XPS spectra (b) of VG, VGP and VGP/Ag.

VG surface contains two elements: C and O. The presence of weak oxygen signal is attributed to surface contamination. The VGP surface contains three elements. The intensity of the O1s peak noticeably increased, and the appearance of the N1s peak suggests successful coating of the VG surface with a PDA layer. In the spectrum of the VGP/Ag, the appearance of Ag3d peak clearly confirmed the successful assembly of Ag nanoparticles. In addition, the high-resolution C1s spectra of VG is shown in Fig. 3a. Two peaks with binding energies of 284.5 and 285.7 eV were observed, corresponding to sp^2 and sp^3 carbon components, respectively. Significantly less intense peaks at 286.9 eV (C—O), 287.8 eV (C=O), and 289.0 eV (O—C=O) were also observed [44,45]. The high-resolution C1s and O1s spectra of VGP is shown in Fig. 3b and c. The C1s spectra were analyzed to identify distinct components with binding energies 284.6, 286.2, 287.8, 288.9, and 290.9 eV, representing C—C, C—N, C—O, C=O, and π - π bonds, respectively. The O1s spectra were deconvoluted into two components assigned to O=C (531.0 eV) and O—C (532.9 eV) species, respectively [46]. The high-resolution spectra of VGP/Ag, shown in Fig. 3, exhibit the core level spectrum of Ag3d, with signals at binding energies of 368.2 and 374.2 eV corresponding to $Ag3d_{5/2}$ and $Ag3d_{3/2}$ of metallic silver (Fig. 3f). In Fig. 3d, the C1s spectrum revealed a ratio of quinone species (C=O) to hydroxyl groups (C—O) of 0.71 in VGP, contrasting with a value of 1.14 in VGP/

Ag, indicating an increase in quinone and a decrease in phenolic hydroxyl after reaction. This observation was further supported by O1s spectra in Fig. 3e, where the ratio of quinone species (O=C) to hydroxyl groups (O—C) rose from 0.41 to 1.16 following the reaction. This suggests that Ag^+ ions were reduced to metallic nanoparticles because of the presence of catechol groups of PDA surfaces, which is consistent with the previous studies [47,48]. The modification of PDA and Ag nanoparticles on VG was studied by FTIR spectra. As shown in Fig. S4, the absorption bands at 2984 and 2902 cm^{-1} belong to the antisymmetric and symmetric stretching vibrations of $-CH_2$ in PDA. The typical peaks located from 1200 to 1700 cm^{-1} are observed in the spectrum of VGP and VGP/Ag, which can be ascribed to stretching vibration of aromatic C=C bonds, carbonyl group and the C—O in the PDA [49].

Sustained release of Ag^+ is expected to achieve a long-term antibacterial property. Fig. 4a shows the Ag^+ release profiles from the VGP/Ag in PBS. Initially, Ag^+ was burst released from the VGP/Ag on the first day. Thereafter, the amounts of released Ag^+ diminished gradually and reached a near steady-state with immersion time, which implied that VGP/Ag went into a sustained Ag^+ release process. In addition, the cumulative release data (inset Fig. 4a) showed a good fit with a pseudo-first-order kinetics models [50,51]. It suggested that the diffusion of Ag^+ through the matrix is rather fast and the overall release is controlled by

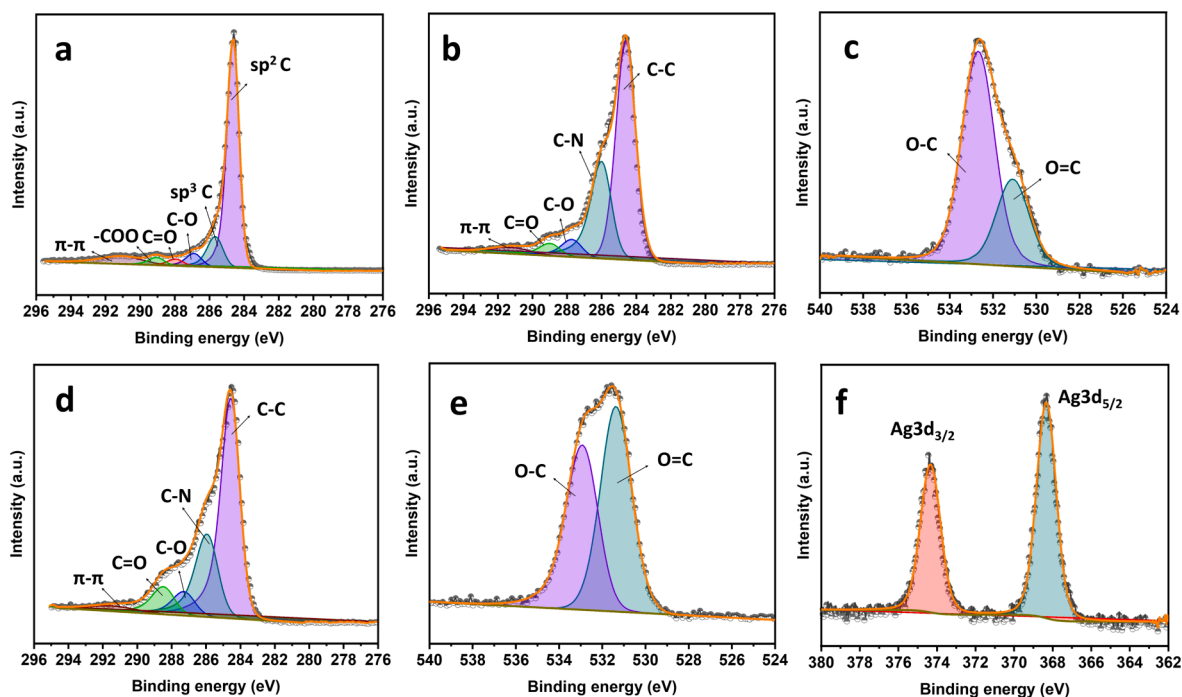


Fig. 3. High-resolution C1s spectrum of VG (a), high-resolution C1s (b) and O1s (c) spectrum of VGP, high-resolution C1s (d) and O1s (e) and Ag3d (f) spectrum of VGP/Ag.

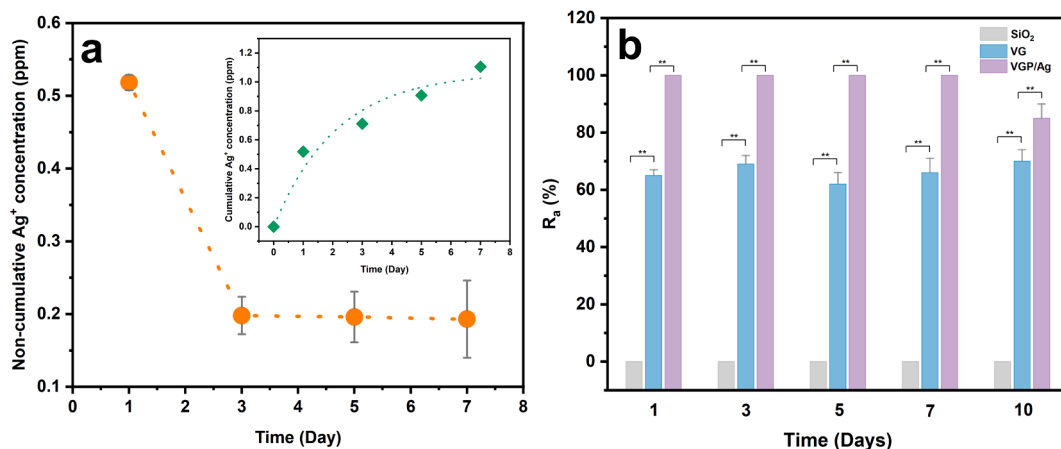


Fig. 4. (a) Non-cumulative and cumulative silver release profiles from VGP/Ag into PBS, (b) Antibacterial activity against *E. coli* on the specimen (R_a). The antibacterial assays data represent mean \pm standard deviation error (** $p < 0.01$).

oxidation and dissolution of the Ag nanoparticles [52].

The antibacterial properties of VG and VGP/Ag were evaluated by colony counting method, with representative Gram-negative bacteria *E. coli*. As shown in Fig. 4b, the antibacterial activity of VG against *E. coli* was approximately 65%. Whereas VGP/Ag exhibited 100% antibacterial activity. This indicates that VGP/Ag has a more advantageous performance compared with VG alone. Furthermore, the antibacterial durability of VGP/Ag was verified after storage in PBS, and the R_a value did not decrease for at least 7 days. After 10 days of storage, the R_a value decreased to approximately 85%, with excellent antibacterial performance against *E. coli*. These findings indicate that VGP/Ag can effectively prevent bacterial colonization on the surface of biomedical devices.

The effectiveness of VGP/Ag in preventing bacterial colonization and biofilm formation was further confirmed through live/dead fluorescence staining, illustrated in Fig. 5a. No dead cells were observed on the SiO₂

wafer. However, propidium iodide staining of bacteria on the VG samples revealed robust red fluorescence signals, indicating a significant portion of dead cells. Conversely, VGP/Ag samples stored in PBS for 7 days showed almost no viable live bacteria. This indicates that the VGP/Ag combination is even more proficient in impeding the bacterial surface colonization. Additionally, bacterial morphological changes were investigated through SEM imaging (Fig. 5b). Consistent with the live/dead staining, SEM analysis revealed a similar trend of antibacterial efficacy. The SiO₂ wafer exhibited a dense biofilm structure with some exopolysaccharide matrix. By contrast, bacteria cells observed on the VG samples showed a significant degree of fracture and deformation, whereas very few cells were observed on the VGP/Ag surfaces. The capability of VGP/Ag to prevent bacterial attachment was challenged through intensive bacterial cultivation. The VGP/Ag species were exposed to bacterial cultures for 5 days, with a bacterial inoculum being introduced every 24 h. The results of this challenge test are shown in

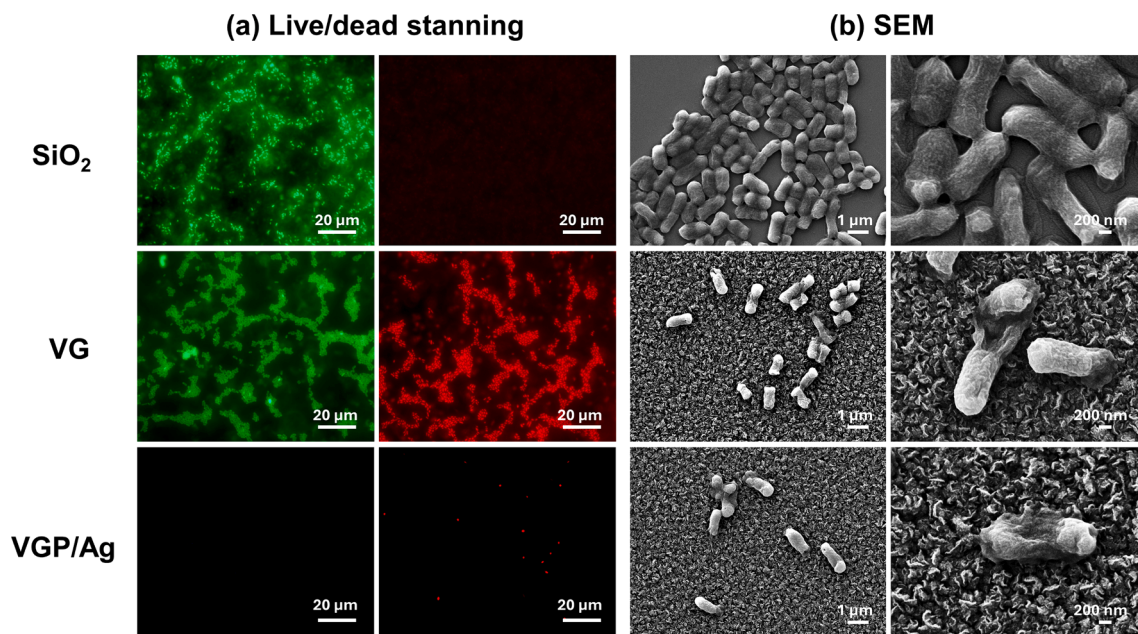


Fig. 5. Representative (a) live/dead fluorescent staining and (b) SEM images showing viability of *E. coli* grown on SiO₂ wafer, VG and VGP/Ag. Green indicates live bacteria and red indicates dead bacteria. (For interpretation of the references to colour in this figure legend, the reader is referred to the web version of this article.)

Fig. S5, revealing a remarkable antibacterial effect of 77.5 % after 5 days. This is significantly higher than the antibacterial activity of VG alone. Biomedical implants are less likely to face such a high bacterial load in real-life situations inside the human body, and this assay was conceived to test the absolute boundaries of the developed coatings. This observation highlights the superiority of the composite VGP/Ag coating used in this study.

Antibacterial coatings with ideal surface structures should demonstrate sustained efficacy in preventing biofilm formation over an extended period. After 24 h of bacterial inoculation, the antibacterial activity of VG against *E. coli* was approximately 65 %, consistent with our previous results [33,35]. The shape of VG nanoflakes is crucial for the antibacterial effect, as the nanoflakes pierce bacterial membranes like thorns, causing mechanical damage, as shown in the SEM images in Fig. 5b. Additionally, VGP/Ag exhibited 100 % antibacterial activity and more effectively prevented bacterial adhesion. The inclusion of Ag nanoparticles enhanced the antibacterial activity. Here, graphene nanoflakes are vertically arranged to form a three-dimensional structure, providing a large surface area and significant capacity to immobilize antibacterial agents [53]. The self-polymerized PDA layer demonstrated stability and strong binding to graphene, chelating and reducing Ag ions. The inherent reducing properties of PDA prevented the oxidative dissolution of Ag nanoparticles and allowed reversible binding to the surrounding Ag ions, resulting in sustained release [54]. The antibacterial activity remained at 100 % after 1 week of storage in PBS buffer. The antibacterial action of Ag nanoparticles operates through Ag ion release or direct contact with bacteria [55,56]. Ag nanoparticles adhere to bacterial membranes through electrostatic attraction, increasing membrane permeability and causing cell lysis. Additionally, the diffusion of Ag ions within cells triggers several effects, including reactive oxygen species (ROS) generation, DNA damage, and inhibition of protein and ribosome functions [57]. On the VGP/Ag surface, the interaction between the VG and cells may facilitate the direct contact between the cell membrane and Ag nanoparticles and the penetration of Ag ions, ensuring high antibacterial activity [58–60].

Notably, after 5 days of continuous exposure to bacterial culture and introducing new bacterial inoculum every 24 h (Fig. S5), the antibacterial effect of VG gradually weakened, while VGP/Ag maintained over 75 % effectiveness. After exposure to a large number of bacteria, the

pure VG were covered by ruptured cells and cell metabolites, indicating physical damage induced by VG nanoarrays occupies a limited contribution in *E. coli* inactivation and weakening the antibacterial effect. The surface of VGP/Ag generated sustained antibacterial microenvironments due to the intervention of Ag nanoparticles, capable of preventing bacterial adhesion and growth over prolonged periods and effectively slowing down biofilm development. While transitioning findings from in vitro studies to the complexities of biofilm infections in vivo presents challenges, this study simulated an exceptionally demanding microbial environment. Notably, the bacterial concentration utilized (10^6 CFU/mL) is much harsher than that typically encountered in vivo, so it is expected that the coatings will translate into very effective in vivo antimicrobial protection [54,61]. The antibacterial properties of VG and Ag nanoparticles decorated vertical nanoarray coatings are summarized in Table S2. The activity of the antibacterial coating is related to the loading capacity of the Ag nanoparticles assembled on the surface [61]. The loading of Ag nanoparticles on the PDA surface depends on factors such as the concentration of Ag ions, reduction time, and temperature [62,63]. The next step will focus on studying the effect of different amounts of Ag nanoparticle loadings on the antibacterial properties of VG coatings.

To examine the biocompatibility of VGP/Ag species, MG-63 osteoblast human cell line was used. Fig. 6a shows a standard alamarBlue assay to quantify cell viability upon a 24 h period of exposure to SiO₂, VG and VGP/Ag. The results obtained showed VG and VGP/Ag were biocompatible, but decreased cell viability to ~94 % ($p > 0.05$) and ~88 % ($p < 0.05$), respectively, versus SiO₂ controls. For the morphology results of cell attachment, the growth patterns of the cells on the samples are presented under SEM in Fig. 6b. MG-63 cells exhibited strong anchorage to both VG and VGP/Ag surfaces. Cells were evenly distributed and displayed abundant stress fibers, forming interconnected networks. Moreover, the cells exhibited polygonal shapes typical of well-stretched osteoblasts, characterized by filamentous structures and intimate contact with the substrate. Quantitatively, there was no significant decrease in surface coverage of the cells adherence (Fig. 6c). Additionally, MG-63 cells were treated with SYTOX Green to indicate the presence of dead cell nuclei within a population. Fig. S6 confirms a homogenous growth of the cells on VG and VGP/Ag surfaces, while almost no dead cell signal was observed. These results indicate

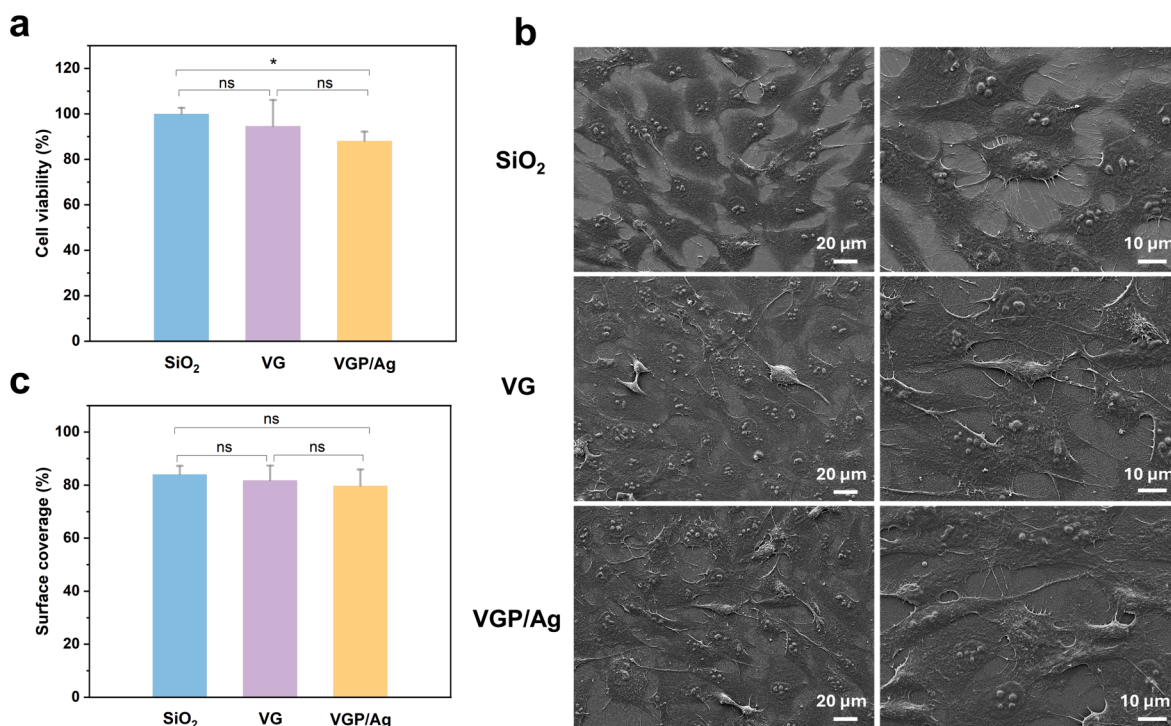


Fig. 6. (a) Cell viability of MG-63 cells after administration of the SiO₂, VG and VGP/Ag; (b) SEM images of MG-63 cells cultured on SiO₂, VG and VGP/Ag; (c) Quantification of the surface coverage of MG-63 cells cultured on SiO₂, VG and VGP/Ag. The data represent mean \pm standard deviation error (* $p < 0.05$, ^{ns} $p > 0.05$).

that VGP/Ag has excellent biocompatibility, which is consistent with the previous reports. The mammalian cells are approximately 20 μm in size. They are an order of magnitude larger than the bacterial cells, which suffered no significant damage when in contact with VG and nanoarray surfaces [35,60]. The biocompatibility of Ag nanomaterials towards eukaryotic cells deserves attention [64]. Free-standing Ag nanoparticles are highly active and tend to freely release Ag⁺ when exposed to water, which can easily cause toxicity to cells. The Ag nanoparticles in this study were anchored on the surface of PDA modified VG, and their mobility was limited. In particular, PDA anchored Ag nanoparticles exhibit relative stability in media, and the Ag⁺ release is slow and gradual. VGP/Ag did not seem to affect cell adhesion but prevented bacterial adhesion, which maybe results from the fact that mammalian cells are more tolerant to Ag⁺ than bacteria [54]. Additionally, the extracellular polymeric substances of MG-63 cells secreted on the surface of Ag nanoparticles can reduce contact-induced Ag⁺ toxicity [65]. Interestingly, PDA has been reported to help achieve rapid surface biomineralization of material surfaces, enhance protein adsorption and cell adhesion, thereby helping to improve the biocompatibility [66].

4. Conclusions

Building on previously reported homogeneous VG coatings [21,36], in this study we developed hybrid VGP/Ag antimicrobial coatings with significant antibacterial properties. The array is fabricated reproducibly by PECVD. Ag nanoparticles were integrated into VG nanospikes, leveraging the adhesion and green reduction capabilities of the PDA layer. This VGP/Ag coating can sustain the release of Ag ions. Our study surpasses previous strategies by combining the physical damage of VG with the antibacterial activity of Ag nanoparticles. The mechanical damage caused by the contact of bacteria with VG facilitates the direct entry of Ag ions into the bacteria, thereby enhancing the overall antibacterial effect. We performed in vitro antimicrobial studies under conditions more stringent than those typically encountered in vivo. Comparative analysis with previous studies showed that VGP/Ag significantly improved the antibacterial ability of VG [33,35]. The

antibacterial activity of VGP/Ag against *E. coli* was 100 %. Even after continuous exposure to bacteria for 5 days, the antibacterial effect of VGP/Ag remained as high as 77.5 %, much higher than that of VG alone. Furthermore, VGP/Ag exhibited minimal biological toxicity, which is promising for subsequent in vivo studies and bio-integration. This long-term antimicrobial effect offers great potential for protecting biomedical implants from bacterial adhesion and subsequent infections. To further develop VGP/Ag coatings, our ongoing studies are more focused on the relationship between Ag nanoparticle loading and antibacterial properties and biocompatibility. This is crucial for translation and long-term evaluation in future clinical practice.

Funding

This work has been financially supported by the Novo Nordisk Foundation (NNF10CC1016517), Nord Forsk (Project no. 105121), Novo Nordisk Foundation (NNF20OC0064547), Vetenskapsrådet (2020-04096) and Chalmers Area of Advance NANO grant.

CRediT authorship contribution statement

Jian Zhang: Writing – review & editing, Writing – original draft, Validation, Methodology, Investigation, Conceptualization. **Santosh Pandit:** Writing – review & editing, Writing – original draft, Supervision, Methodology, Conceptualization. **Shadi Rahimi:** Writing – original draft, Methodology, Investigation. **Zhejian Cao:** Writing – original draft, Methodology, Investigation. **Ivan Mijakovic:** Writing – review & editing, Writing – original draft, Supervision, Funding acquisition, Conceptualization.

Declaration of competing interest

The authors declare that they have no known competing financial interests or personal relationships that could have appeared to influence the work reported in this paper.

Data availability

Data will be made available on request.

Appendix A. Supplementary material

Supplementary data to this article can be found online at <https://doi.org/10.1016/j.jcis.2024.07.173>.

References

- [1] S.L. Percival, L. Suleman, C. Vuotto, G. Donelli, Healthcare-associated infections, medical devices and biofilms: risk, tolerance and control, *J. Med. Microbiol.* 64 (2015) 323–334.
- [2] A. Singh, A. Amod, P. Pandey, P. Bose, M.S. Pingali, S. Shivalkar, P.K. Varadwaj, A. K. Sahoo, S.K. Samanta, Bacterial biofilm infections, their resistance to antibiotics therapy and current treatment strategies, *Biomed. Mater.* 17 (2022) 022003.
- [3] Y. Wu, Y. Long, Q. Li, S. Han, J. Ma, Y. Yang, H. Gao, Layer-by-layer (LBL) self-assembled biohybrid nanomaterials for efficient antibacterial applications, *ACS Appl. Mater. Interfaces* 7 (2015) 17255–17263.
- [4] H.Y. Ahmadabadi, K. Yu, J.N. Kizhakkedathu, Surface modification approaches for prevention of implant associated infections, *Colloids Surf. B Biointerfaces* 193 (2020) 111116.
- [5] A. Balestri, J. Cardellini, D. Berti, Gold and silver nanoparticles as tools to combat multidrug-resistant pathogens, *Curr. Opin. Colloid Interface Sci.* 66 (2023) 101710.
- [6] M. Su, W. Zhou, L. Liu, M. Chen, Z. Jiang, X. Luo, Y. Yang, T. Yu, W. Lei, C. Yuan, Micro eddy current facilitated by screwed MoS₂ structure for enhanced hydrogen evolution reaction, *Adv. Funct. Mater.* 32 (2022) 2111067.
- [7] Z. Xiong, C. Hu, X. Luo, W. Zhou, Z. Jiang, Y. Yang, T. Yu, W. Lei, C. Yuan, Field-free improvement of oxygen evolution reaction in magnetic two-dimensional heterostructures, *Nano Lett.* 21 (2021) 10486–10493.
- [8] W. Zhou, M. Chen, M. Guo, A. Hong, T. Yu, X. Luo, C. Yuan, W. Lei, S. Wang, Magnetic enhancement for hydrogen evolution reaction on ferromagnetic MoS₂ Catalyst, *Nano Lett.* 20 (2020) 2923–2930.
- [9] W. He, L. Zhou, M. Wang, Y. Cao, X. Chen, X. Hou, Structure development of carbon-based solar-driven water evaporation systems, *Sci. Bull.* 66 (2021) 1472–1483.
- [10] X. Wei, F. Yan, Q. Lv, W. Zhu, C. Hu, A. Patané, K. Wang, Enhanced photoresponse in MoTe₂ photodetectors with asymmetric graphene contacts, *Adv. Opt. Mater.* 7 (2019) 1900190.
- [11] T. Hu, X. Mei, Y. Wang, X. Weng, R. Liang, M. Wei, Two-dimensional nanomaterials: fascinating materials in biomedical field, *Sci. Bull.* 64 (2019) 1707–1727.
- [12] Z. Zhu, H. Luo, T. Wang, C. Zhang, M. Liang, D. Yang, M. Liu, W.W. Yu, Q. Bai, L. Wang, N. Sui, Plasmon-enhanced peroxidase-like activity of nitrogen-doped graphdiyne oxide quantum dots/gold-silver nanocage heterostructures for antimicrobial applications, *Chem. Mater.* 34 (2022) 1356–1368.
- [13] D. Dai, D. Zhou, H. Xie, J. Wang, C. Zhang, The design, construction and application of graphene family composite nanocoating on dental metal surface, *Biomater. Adv.* (2022) 213087.
- [14] J. Zhang, P. Singh, Z. Cao, S. Rahimi, S. Pandit, I. Mijakovic, Polydopamine/graphene oxide coatings loaded with tetracycline and green Ag nanoparticles for effective prevention of biofilms, *Appl. Surf. Sci.* 626 (2023) 157221.
- [15] S. Pandit, K. Gaska, R. Kádár, I. Mijakovic, Graphene-based antimicrobial biomedical surfaces, *ChemPhysChem* 22 (2021) 250–263.
- [16] A.N. Obraztsov, Making graphene on a large scale, *Nat. Nanotechnol.* 4 (2009) 212–213.
- [17] Y. Zhang, L. Zhang, C. Zhou, Review of chemical vapor deposition of graphene and related applications, *Acc. Chem. Res.* 46 (2013) 2329–2339.
- [18] L. Dellieu, E. Lawaree, N. Reckinger, C. Didembourg, J.J. Letesson, M. Sarrazin, O. Deparis, J.Y. Matroule, J.F. Colomer, Do CVD grown graphene films have antibacterial activity on metallic substrates, *Carbon* 84 (2015) 310–316.
- [19] J. Shao, W. Lv, Q. Yang, Self-assembly of graphene oxide at interfaces, *Adv. Mater.* 26 (2014) 5586–5612.
- [20] J. Sun, T. Rattanasawatessun, P. Tang, Z. Bi, S. Pandit, L. Lam, C. Wasén, M. Erlandsson, M. Bokarewa, J. Dong, F. Ding, F. Xiong, I. Mijakovic, Insights into the mechanism for vertical graphene growth by plasma-enhanced chemical vapor deposition, *ACS Appl. Mater. Interfaces* 14 (2022) 7152–7160.
- [21] A. Al-Jumaili, M.A. Zafar, K. Bazaka, J. Weerasinghe, M.V. Jacob, Bactericidal vertically aligned graphene networks derived from renewable precursor, *Carbon Trends* 7 (2022) 100157.
- [22] X. Lu, X. Feng, J.R. Werber, C. Chu, I. Zucker, J.H. Kim, C.O. Osuji, M. Elimelech, Enhanced antibacterial activity through the controlled alignment of graphene oxide nanosheets, *Proc. Nat. Acad. Sci.* 114 (2017) 9793–9801.
- [23] O. Akhavan, E. Ghaderi, Toxicity of graphene and graphene oxide nanowalls against bacteria, *ACS Nano* 4 (2010) 5731–5736.
- [24] X. Zou, L. Zhang, Z. Wang, Y. Luo, Mechanisms of the antimicrobial activities of graphene materials, *J. Am. Chem. Soc.* 138 (2016) 2064–2077.
- [25] G. Cao, J. Yan, X. Ning, Q. Zhang, Q. Wu, L. Bi, Y. Zhang, Y. Han, J. Guo, Antibacterial and antibiofilm properties of graphene and its derivatives, *Colloids Surf. B Biointerfaces* 200 (2021) 111588.
- [26] A. Radhi, D. Mohamad, F.S.A. Rahman, A.M. Abdullah, H. Hasan, Mechanism and factors influence of graphene-based nanomaterials antimicrobial activities and application in dentistry, *J. Mater. Res. Technol.* 11 (2021) 1290–1307.
- [27] O.N. Ruiz, K.A.S. Fernando, B. Wang, N.A. Brown, P.G. Luo, N.D. McNamara, M. Vangsnest, Y. Sun, C.E. Bunker, *ACS Nano* 5 (2011) 8100–8107.
- [28] C. Zhao, S. Pandit, Y. Fu, I. Mijakovic, A. Jesorka, J. Liu, Graphene oxide based coatings on nitinol for biomedical implant applications: effectively promote mammalian cell growth but kill bacteria, *RSC Adv.* 6 (2016) 38124–38134.
- [29] Y. Tu, M. Lv, P. Xiu, T. Huynh, M. Zhang, M. Castelli, Z. Liu, Q. Huang, C. Fan, H. Fang, R. Zhou, Destructive extraction of phospholipids from *Escherichia coli* membranes by graphene nanosheets, *Nat. Nanotechnol.* 8 (2013) 594–601.
- [30] Q. Xin, H. Shah, A. Nawaz, W. Xie, M.Z. Akram, A. Batool, L. Tian, S.U. Jan, R. Boddula, B. Guo, Q. Liu, J. Gong, Antibacterial carbon-based nanomaterials, *Adv. Mater.* 31 (2019).
- [31] K. Krishnamoorthy, M. Veerapandian, L. Zhang, K. Yun, S.J. Kim, Antibacterial efficiency of graphene nanosheets against pathogenic bacteria via lipid peroxidation, *J. Phys. Chem. C* 116 (2012) 17280–17287.
- [32] S. Liu, T.H. Zeng, M. Hofmann, E. Burcombe, J. Wei, R. Jiang, J. Kong, Y. Chen, Antibacterial activity of graphite graphite oxide, graphene oxide, and reduced graphene oxide: membrane and oxidative stress, *ACS Nano* 5 (2011) 6971–6980.
- [33] Y. Chen, S. Pandit, S. Rahimi, I. Mijakovic, Graphene nanospikes exert bactericidal effect through mechanical damage and oxidative stress, *Carbon* 218 (2024) 118740.
- [34] W. Wei, J. Li, Z. Liu, Y. Deng, D. Chen, P. Gu, G. Wang, X. Fan, Distinct antibacterial activity of a vertically aligned graphene coating against Gram-positive and Gram-negative bacteria, *J. Mater. Chem. B* 8 (2020) 6069–6079.
- [35] S. Pandit, Z. Cao, V.R.S.S. Mokkaapati, E. Celauro, A. Yurgens, M. Lovmar, F. Westerlund, J. Sun, I. Mijakovic, Vertically aligned graphene coating is bactericidal and prevents the formation of bacterial biofilms, *Adv. Mater. Interfaces* 5 (2018).
- [36] X. Zhang, J. Qiu, J. Tan, D. Zhang, L. Wu, Y. Qiao, G. Wang, J. Wu, K.W.K. Yeung, X. Liu, In-situ growth of vertical graphene on titanium by PECVD for rapid sterilization under near-infrared light, *Carbon* 192 (2022) 209–218.
- [37] H. Lee, S.M. Dellatore, W.M. Miller, P.B. Messersmith, Mussel-inspired surface chemistry for multifunctional coatings, *Science* 318 (2007) 426–430.
- [38] T.G. Barclay, H.M. Hegab, S.R. Clarke, M. Ginic-Markovic, Versatile surface modification using polydopamine and related polycatecholamines: chemistry structure, and applications, *Adv. Mater. Interfaces* 4 (2017).
- [39] L. Deng, Y. Deng, K. Xie, AgNPs-decorated 3D printed PEEK implant for infection control and bone repair, *Colloids Surf. B Biointerfaces* 160 (2017) 483–492.
- [40] J. Han, Y. Ma, M. Wang, L. Li, Z. Tong, L. Xiao, S. Jia, X. Chen, Oxygen-assisted trimming growth of ultrahigh vertical graphene films in a PECVD process for superior energy storage, *ACS Appl. Mater. Interfaces* 13 (2021) 12400–12407.
- [41] J. Ma, M. Zhang, W. Su, B. Wu, Z. Yang, X. Wang, B. Qiao, H. Pei, J. Tu, D. Chen, Q. Wu, Photoelectrochemical enzyme biosensor based on TiO₂ nanorod/TiO₂ quantum dot/polydopamine/glucose oxidase composites with strong visible-light response, *Langmuir* 38 (2022) 751–761.
- [42] S. Xu, S. Wang, Z. Chen, Y. Sun, Z. Gao, H. Zhang, J. Zhang, Electric-field-assisted growth of vertical graphene arrays and the application in thermal interface materials, *Adv. Funct. Mater.* 30 (2020).
- [43] C. Karupppiah, K. Venkatesh, L. Hsu, P. Arunachalam, C. Yang, S.K. Ramaraj, R. J. Ramalingam, S. Arokiyaraj, H.A. Al-Lohedan, An improving aqueous dispersion of polydopamine functionalized vapor grown carbon fiber for the effective sensing electrode fabrication to chloramphenicol drug detection in food samples, *Microchem. J.* 170 (2021) 106675.
- [44] G. Sahoo, S. Ghosh, S.R. Polaki, T. Mathews, M. Kamruddin, Scalable transfer of vertical graphene nanosheets for flexible supercapacitor applications, *Nanotechnology* 28 (41) (2017) 415702.
- [45] P. Ji, J. Chen, T. Huang, C. Jin, L. Zhuge, X. Wu, Fast preparation of vertical graphene nanosheets by helicon wave plasma chemical vapor deposition and its electrochemical performance, *Diam. Relat. Mater.* 108 (2020) 107958.
- [46] K.G. Malollari, P. Delparastan, C. Sobek, S.J. Vachhani, T.D. Fink, R.H. Zha, P. B. Messersmith, Mechanical enhancement of bioinspired polydopamine nanocoatings, *ACS Appl. Mater. Interfaces* 11 (46) (2019) 43599–43607.
- [47] F. Wei, J. Liu, Y. Zhu, X. Wang, C. Cao, W. Song, In situ facile loading of noble metal nanoparticles on polydopamine nanospheres via galvanic replacement reaction for multifunctional catalysis, *Sci. China Chem.* 60 (2017) 1236–1242.
- [48] X. He, T. Zhu, H. Mao, L. Cai, Chitin Whisker/dopamine enhancing in-situ generation of silver nanoparticles for fabricating functional silk fabrics, *Fibers Polym.* 24 (5) (2023) 1649–1660.
- [49] K. Chen, Q. Tian, C. Tian, G. Yan, F. Cao, S. Liang, X. Wang, Mechanical reinforcement in thermoplastic polyurethane nanocomposite incorporated with polydopamine functionalized graphene nanoplatelet, *Ind. Eng. Chem. Res.* 56 (41) (2017) 11827–11838.
- [50] F.M. Silva, R.J.B. Pinto, A.L. Daniel-da-Silva, T. Trindade, Cationic release behavior of antimicrobial cellulose/silver nanocomposites, *Cellul.* 21 (2014) 3551–3560.
- [51] D. Phan, N. Dorjjugder, Y. Saito, G. Taguchi, A. Ullah, D. Kharaghani, I. Kim, The synthesis of silver-nanoparticle-anchored electrospun polyacrylonitrile nanofibers and a comparison with as-spun silver/polyacrylonitrile nanocomposite membranes upon antibacterial activity, *Polym. Bull.* 77 (2020) 4197–4212.
- [52] K. Chen, K. Xie, Q. Long, L. Deng, Z. Fu, H. Xiao, L. Xie, Fabrication of core-shell Ag@pDA@HAP nanoparticles with the ability for controlled release of Ag⁺ and superior hemocompatibility, *RSC Adv.* 7 (2017) 29368–29377.

- [53] W. Xiao, B. Li, J. Yan, L. Wang, X. Huang, J. Gao, Three dimensional graphene composites: preparation, morphology and their multi-functional applications, *Compos. A Appl. Sci. Manuf.* 165 (2023) 107335.
- [54] Z. Jia, P. Xiu, P. Xiong, W. Zhou, Y. Cheng, S. Wei, Y. Zheng, T. Xi, H. Cai, Z. Liu, C. Wang, W. Zhang, Z. Li, Additively manufactured macroporous titanium with silver-releasing micro-/nanoporous surface for multipurpose infection control and bone repair -a proof of concept, *ACS Appl. Mater. Interfaces* 8 (2016) 28495–28510.
- [55] J.S. Kim, E. Kuk, K.N. Yu, J.H. Kim, S.J. Park, H.J. Lee, S.H. Kim, Y.K. Park, Y. H. Park, C.Y. Hwang, Y.K. Kim, Y.S. Lee, D.H. Jeong, M.H. Cho, Antimicrobial effects of silver nanoparticles, *Nanomed. Nanotechnol. Biol. Med.* 3 (2007) 95–101.
- [56] P.R.A. Claro, R.T. Konatu, A.L. do Amaral Escada, M.C. de Souza Nunes, C. V. Maurer-Morelli, M.F. Dias-Netipanyj, K.C. Popat, D. Mantovani, Incorporation of silver nanoparticles on Ti7.5Mo alloy surface containing TiO₂ nanotubes arrays for promoting antibacterial coating - In vitro and in vivo study, *Appl. Surf. Sci.* 455 (2018) 780–788.
- [57] P. Singh, I. Mijakovic, Antibacterial effect of silver nanoparticles is stronger if the production host and the targeted pathogen are closely related, *Biomedicines* 10 (2022) 628.
- [58] A. Costas, N. Preda, I. Zgura, A. Kuncser, N. Apostol, C. Curutiu, I. Enculescu, Silver nanoparticles decorated ZnO-CuO core-shell nanowire arrays with low water adhesion and high antibacterial activity, *Sci. Rep.* 13 (2023) 10698.
- [59] G. Liu, Z. Hu, X. Chen, W. Li, Y. Wu, Z. Liu, L. Miao, Z. Luo, J. Wang, Y. Guo, Oxygen vacancy-rich Ag/CuO nanoarray mesh fabricated by laser ablation for efficient bacterial inactivation, *J. Hazard. Mater.* 465 (2024) 133269.
- [60] L. Victor, Y. Chen, E. Naumovska, S. Pandit, E. Schröder, I. Mijakovic, S. Rahimi, Differences in interaction of graphene/graphene oxide with bacterial and mammalian cell membranes, *Nanoscale* 16 (2024) 1156–1166.
- [61] L. Zhao, H. Wang, K. Huo, L. Cui, W. Zhang, H. Ni, Y. Zhang, Z. Wu, P.K. Chu, Antibacterial nano-structured titania coating incorporated with silver nanoparticles, *Biomaterials* 32 (2011) 5706–5716.
- [62] L. Zhang, Z. Liu, Y. Wang, R. Xie, X. Ju, W. Wang, L. Lin, L. Chu, Facile immobilization of Ag nanoparticles on microchannel walls in microreactors for catalytic applications, *Chem. Eng. J.* 309 (2017) 691–699.
- [63] H. Niu, S. Wang, T. Zeng, Y. Wang, X. Zhang, Z. Meng, Y. Cai, Preparation and characterization of layer-by-layer assembly of thiols/Ag nanoparticles/polydopamine on PET bottles for the enrichment of organic pollutants from water samples, *J. Mater. Chem.* 22 (2012) 15644–15653.
- [64] P.V. AshaRani, G.L.K. Mun, M.P. Hande, S. Valiyaveetil, Cytotoxicity and genotoxicity of silver nanoparticles in human cells, *ACS Nano* 3 (2009) 279–290.
- [65] Z. Jia, P. Xiu, M. Li, X. Xu, Y. Shi, Y. Cheng, S. Wei, Y. Zheng, T. Xi, H. Cai, Z. Liu, Bioinspired anchoring AgNPs onto micro-nanoporous TiO₂ orthopedic coatings: trap-killing of bacteria, surface-regulated osteoblast functions and host responses, *Biomaterials* 75 (2016) 203–222.
- [66] J. Ryu, S.H. Ku, H. Lee, C.B. Park, Mussel-inspired polydopamine coating as a universal route to hydroxyapatite crystallization, *Adv. Funct. Mater.* 20 (2010) 2132–2139.